Accepted Manuscript

Facile Hydrothermal Growth Graphene/ZnO Nanocomposite for Development of Enhanced Biosensor

Sze Shin Low, Michelle T.T. Tan, Hwei-San Loh, Poi Sim Khiew, Wee Siong Chiu

PII: S0003-2670(15)01365-3

DOI: 10.1016/j.aca.2015.11.006

Reference: ACA 234245

To appear in: *Analytica Chimica Acta*

Received Date: 26 April 2015

Revised Date: 16 October 2015

Accepted Date: 9 November 2015

Please cite this article as: S.S. Low, M.T.T. Tan, H.-S. Loh, P.S. Khiew, W.S. Chiu, Facile Hydrothermal Growth Graphene/ZnO Nanocomposite for Development of Enhanced Biosensor, *Analytica Chimica Acta* (2015), doi: 10.1016/j.aca.2015.11.006.

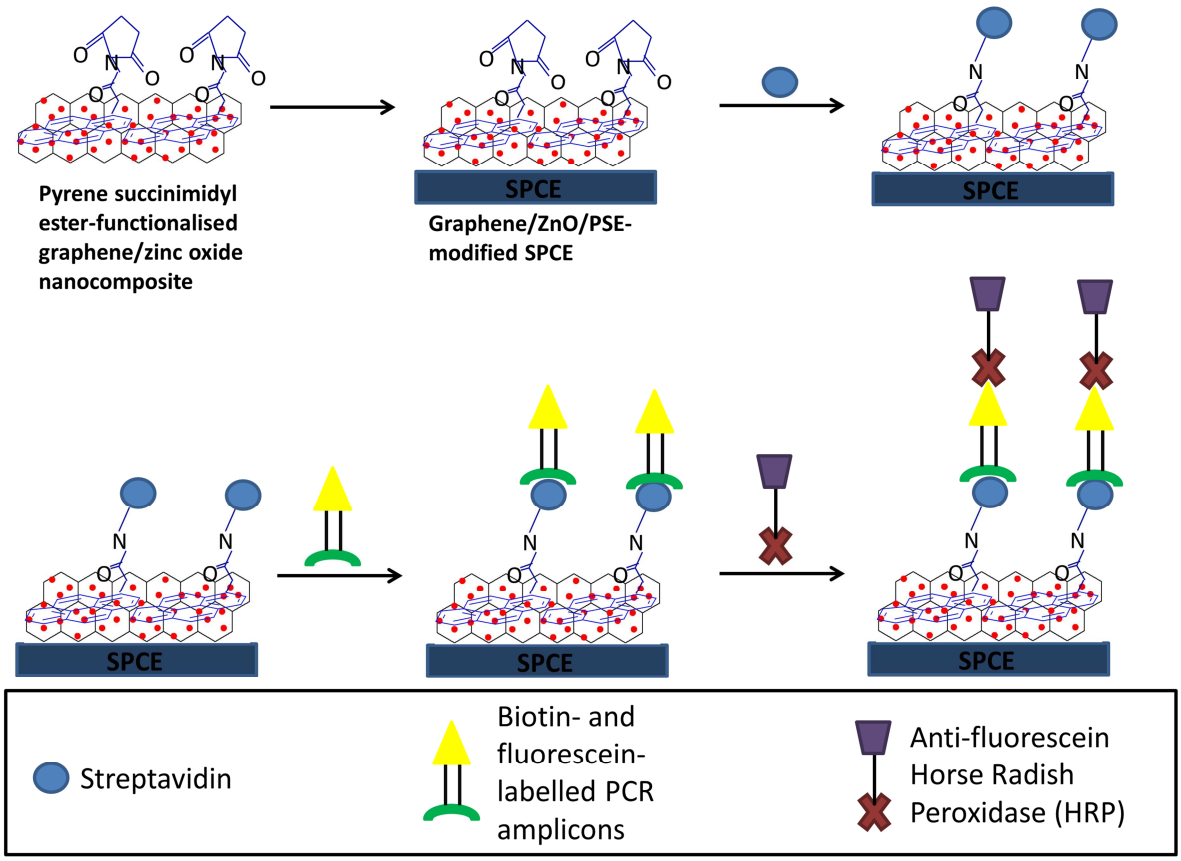
Pyrene succinimidyl ester-functionalised graphene/zinc oxide nanocomposite
Graphene/ZnO/PSE-modified SPCE
SPCE
SPCE
SPCE
SPCE
SPCE
Streptavidin
Biotin- and fluorescein-labelled PCR amplicons
Anti-fluorescein Horse Radish Peroxidase (HRP)

Facile Hydrothermal Growth Graphene/ZnO Nanocomposite for Development of Enhanced Biosensor

Sze Shin Low[a], Michelle T. T. Tan[a,*], Hwei-San Loh[b,c], Poi Sim Khiew[a], Wee Siong Chiu[d]

[a] Department of Electrical and Electronic Engineering, Faculty of Engineering, University of Nottingham Malaysia Campus, Jalan Broga, 43500 Semenyih, Selangor, Malaysia

[b] School of Biosciences, Faculty of Science, University of Nottingham Malaysia Campus, Jalan Broga, 43500 Semenyih, Selangor, Malaysia

[c] Biotechnology Research Centre, University of Nottingham Malaysia Campus, Jalan Broga, 43500 Semenyih, Selangor, Malaysia

[d] Low Dimensional Materials Research Center, Department of Physics, Faculty of Science, University Malaya, 50603 Kuala Lumpur, Malaysia

Abstract

Graphene/zinc oxide nanocomposite was synthesised via a facile, green and efficient approach consisted of novel liquid phase exfoliation and solvothermal growth for sensing application. Highly pristine graphene was synthesised through mild sonication treatment of graphite in a mixture of ethanol and water at an optimum ratio. The X-ray diffractometry (XRD) affirmed the hydrothermal growth of pure zinc oxide nanoparticles from zinc nitrate hexahydrate precursor. The as-prepared graphene/zinc oxide (G/ZnO) nanocomposite was characterised comprehensively to evaluate its morphology, crystallinity, composition and purity. All results clearly indicate that zinc oxide particles were homogenously distributed on graphene sheets, without any severe aggregation. The electrochemical performance of graphene/zinc oxide nanocomposite-modified screen-printed carbon electrode (SPCE) was evaluated using cyclic voltammetry (CV) and amperometry analysis. The resulting electrode exhibited excellent electrocatalytic activity towards the reduction of hydrogen peroxide (H_2O_2) in a linear range of 1 to 15 mM with a correlation coefficient of 0.9977. The sensitivity of the

graphene/zinc oxide nanocomposite-modified hydrogen peroxide sensor was 3.2580 μAmM^{-1} with a limit of detection of 7.4357 μM. An electrochemical DNA sensor platform was then fabricated for the detection of Avian Influenza *H5* gene based on graphene/zinc oxide nanocomposite. The results obtained from amperometry study indicate that the graphene/zinc oxide nanocomposite-enhanced electrochemical DNA biosensor is significantly more sensitive ($P < 0.05$) and efficient than the conventional agarose gel electrophoresis.

Keywords: Graphene/zinc oxide nanocomposite; Green approach; Avian influenza virus H5N1; Hydrogen peroxide; Electrochemical DNA biosensor; Screen printed carbon electrode

1. Introduction

Rapid and accurate detection of causative pathogen is essential in determining the choice of treatment in acute-care settings. Therefore, it is highly desirable for the development of electrochemical biosensor, a small device employing biochemical molecular recognition properties as the basis of a selective analysis. Such devices produce a simple, inexpensive and yet accurate and sensitive platform for patient diagnosis. Extensive research on new sensing concepts, coupled with nanomaterials, has opened the door to widespread clinical applications of electrochemical biosensors [1]. The high sensitivity, specificity, simplicity and inherent miniaturisation of modern electrochemical devices with the enhancement of nanomaterials have been fabricated for the development of nanomaterial-based biosensor for early and efficient detection of diseases.

Graphene, a 2D planar single sheet of sp^2 hybridised carbon atoms arranged in a honeycomb lattice was first discovered by Novoselov and colleagues in 2004 [2]. It is highly anticipated to be an excellent electrode material due to its notable characteristics, such as excellent electrical conductivity, rapid electron mobility, high surface area to volume ratio, good thermal and electrochemical properties [3]. In view of the excellent properties of graphene, development of graphene-based metal oxide composite has been expected to

provide groundbreaking endeavour in a wide variety of application as it will generate composite with desired properties. Particularly, zinc oxide (ZnO), a II-VI compound semiconductor with wide direct band gap of 3.37 eV at room temperature and large exciton binding energy of 60 meV has significant applications in electronic and optoelectronic devices. In addition, ZnO is a biocompatible, biosafe and biodegradable material with a high isoelectric point (IEP) of about 9.5, making it suitable for the absorption of low IEP proteins through electrostatic interaction.

In view of the outstanding individual properties of graphene and ZnO as electrode material, the graphene/ZnO (G/ZnO) composite may exhibit unique intriguing properties due to the synergistic effect between graphene and ZnO for improved electrical conductivity and electron transfer rate. The attracting properties of graphene/ZnO composite has been reported like enhanced photocatalytic performance, energy storage capability, sensing property, optoelectronic property and ultrafast nonlinear optical switching ability [4-8]. Many synthesis routes have been developed for the hybridisation of graphene and ZnO nanoparticles, for example, thermal decomposition, electrochemical deposition, ultrasonic spray pyrolysis and electrohydrodynamic atomisation [9-12]. However, most of the synthesis method used harsh and toxic chemicals to chemically reduce graphene oxide, culminating in the generation of oxygenated functional group on the reduced graphene oxide. These impurities will affect the superior electrical conductivity of the graphene. Therefore, safer synthesis method is crucial to fully harvest the remarkable property of graphene for the production of G/ZnO composite material with optimal synergistic properties.

In this work, an economical and safe method via one step facile solvent exfoliation was used to synthesise the graphene material prior to the incorporation of ZnO precursor for the production of G/ZnO via a low temperature solvothermal synthesis method. The proposed method ensures the preservation of the pristine quality of graphene, in addition to being safer and more economical to produce the G/ZnO nanocomposite material. The structural and physical properties of G/ZnO nanocomposite were evaluated using scanning electron

microscopy (SEM), transmission electron microscopy (TEM), X-ray diffractometry (XRD) and Raman spectroscopy. The potential of the material as electrode platform for electrochemical sensors and its sensitivity towards hydrogen peroxide (H_2O_2), a common by-product of oxidase catalysed reactions were evaluated. An electrochemical DNA biosensor for the detection of Avian Influenza *H5* gene was then fabricated, demonstrating the feasibility of the G/ZnO platform for biosensing applications. The potential of the material as electrode platform for electrochemical sensors was also evaluated via statistical analysis.

2. Experimental

2.1 Materials

Graphite flakes (99% carbon purity) were purchased from Bay Carbon (Michigan, USA). Zinc nitrate hexahydrate $Zn(NO_3)_2 \cdot 6H_2O$ (98% reagent grade), streptavidin (purified from *Streptomyces avidinii*), ethanolamine hydrochloride, bovine serum albumin (BSA), sodium dodecyl sulphate (SDS), sodium chloride (NaCl), monosodium phosphate (NaH_2PO_4), disodium phosphate (Na_2HPO_4), uric acid, fructose, glucose and 1-Pyrenebutyric acid *N*-hydroxysuccinimide ester (PSE) were bought from Sigma Aldrich (St. Louis, USA). Ethanol was obtained from Merck, hydrogen peroxide (H_2O_2, 30%) was purchased from R&M Chemical. 10x saline sodium citrate (SSC) was obtained from First Base (Selangor, Malaysia). All chemicals were used as received and deionized water (DI) from the Millipore system was used throughout the experiment. Phosphate buffer solution (PBS) tables were purchased from Sigma Aldrich and dissolved in DI water to produce 0.1 M buffer solution with pH of 7.4.

2.2 Synthesis of Graphene

Graphene flakes were prepared via a facile green sonochemical approach with graphite as the starting material [13]. Typically, raw graphite flakes were dispersed in mixture of ethanol and DI water (2:3 ratio) and sonication treatment was carried out with a working frequency of 50/60 Hz for 3 hours at room temperature. A darkish black suspension was obtained and

subjected to centrifugation at 1000 rpm for 30 minutes to remove unexfoliated aggregates. The supernatant was dried at 80 ℃ overnight and gr aphene was collected.

2.3 Synthesis of Graphene/ZnO Nanocomposite

Graphene/ZnO nanocomposite was prepared through one step green low temperature hydrothermal growth[14]. The as-synthesised graphene was re-dispersed in ethanol via sonication for 30 minutes. Zinc nitrate hexahydrate (ratio 8:1 with graphene) was added into the graphene dispersion and stirred for 15 minutes to achieve even mixing. Diluted sodium hydroxide (NaOH) solution was added to adjust the mixture to a pH value of 12. The mixture was then transferred to a 50 ml Teflon stainless steel autoclave and heated at 90 ℃ for 10 hours. The supernatant was removed by centrifugation and the solid precipitates were washed repeatedly with excess ethanol and water, respectively, and dried overnight at 80 ℃ to collect the graphene/ZnO nanocomposite.

2.4 Instrumentations and Characterisations

The surface morphology and elemental composition of the samples were analysed using scanning electron microscope (SEM) (FEI Quanta-400 FESEM) and transmission electron microscope (TEM) (JEOL JEM-2100F) at an operating voltage of 200 kV. The crystallographic structure of the samples were investigated using X-ray diffractometer (XRD) (X'pert Pro Powder, PANalytical) using a scanning rate of 0.02 θs^{-1} in a 2θ range of 10-80° with Cu Kα radiation at λ = 1.5406 Å.

2.5 Electrochemical Measurements of Hydrogen Peroxide

The electrochemical performance of the as-synthesised graphene and graphene/ZnO nanocomposite in connection with cyclic voltammetry (CV) were analysed using μAutolab PGSTAT 204 potentiostat (Metrohm, Netherlands). Cyclic voltammograms were recorded from -0.5 V to 0.8 V at a scan rate of 50 mV/s.

2.6 Polymerase Chain Reaction (PCR)

The *H5* DNA sequences of H5N1 strain A/chicken/Malaysia/5744/2004(H5N1) was synthesised based on the Influenza Virus Resource at National Centre for Biotechnology Information (NCBI) (Genbank accession: KC684446). The modified biotin- and fluorescein-labelled primers were designed flanking the *H5* gene and custom synthesised by First Base (Selangor, Malaysia).

Polymerase chain reaction (PCR) was performed using GS2 PCR thermal cycler (G-Storm, UK). Reactions were performed with 0.3 µM of each primer: biotin-modified forward primer, HAFP (B): 5'- /5BiosG/GG TTA CCA TGC AAA CAA CTC GAC AGA GC -3' and fluorescein-modified reverse primer, HARP (F): 5'- /5FluorT/AT TGT AAC GAC CCA TTG GAG CAC ATC CAT AAG -3', with 1x KCl PCR buffer, 1.5 mM $MgCl_2$, 0.3 mM dNTPs and *Taq* polymerase (Fermentas, Lithuania) The DNA template was pre-denatured at 94 ℃ for 3 minutes, amplified for 30 cycles with denaturation at 94 ℃ for 1 minute, annealing at 56.5 ℃ for 1 minute and extension at 72 ℃ for 1 minute 30 seconds with a final elongation at 72 ℃ for 8 minutes.

The PCR amplicons were purified using GeneAll® PCR SV purification kit (GeneAll Biotechnology, Seoul, Korea) and eluted using buffer EB (10 mM TrisCl, pH 8.5) for maximum DNA recovery and long term storage.

2.7 Gel Electrophoresis

PCR amplicons with different dilution factors along with GeneRuler^{TM} 1kb DNA ladder (Fermentas, Lithuania) were subjected to 1% agarose gel electrophoresis. The gel was run at 90 V for 35 minutes, which was then visualised by UV light box and Alpha Innotech Fluorescence (Alpha Innotech, USA).

2.8 Dot Blot Assay

The dot blot assay was carried out in a way similar to the preparation of sandwich platform as shown in Figure 1. Streptavidin (3 µL) was pipetted onto 1 cm^2 of nitrocellulose membrane strip (Bio-Rad, Hercules, CA) and the membrane was subsequently placed in

individual wells of a MicroWell™ 24-well polystyrene plate (Sigma Aldrich) placed on an orbital shaker. PBST buffer (500 µL, 10 minutes) was used for washing after every incubation step unless stated otherwise. Blocking of non-specific antibodies binding was done by incubation with BSA (500 µL, 1 hour). Purified *H5* PCR amplicons (2 µL, different dilutions) were spotted onto the streptavidin-blotted nitrocellulose membrane, followed by anti-fluorescein horseradish peroxidase (HRP) conjugate (2 µL, 30 minutes). The washing step was repeated thrice with PBST for complete removal of unbound conjugates, once with deionised water for removal of buffer residues. Lastly, TMB (300 µL, 5 minutes) was added to the membrane. The reactions were terminated immediately with deionised water, once visible blue aggregates were spotted on the membrane.

2.9 Fabrication of Graphene/ZnO/PSE-Modified Genosensor

The as-synthesised graphene/ZnO nanocomposite and pyrene succinimide ester (PSE) (ratio 1:4) were dispersed in ethanol via sonication for 30 minutes [15]. The mixture was centrifuged at 1000 rpm and washed repeatedly with ethanol and DI water respectively. The sediment was dried overnight at 80 ℃ to collect PSE-functionalized graphene/ZnO nanocomposite (G/ZnO/PSE). 5 µL of the G/ZnO/PSE dispersion was dropped onto the screen printed carbon electrode (SPCE, DropSens, Spain) and air-dried.

The enzyme-based electrochemical genosensor was fabricated using the G/ZnO/PSE-modified electrode as shown in Figure 1. Typically, 5 µL of streptavidin was dropped onto the SPCE and incubated, then 50 µL of ethanolamine hydrochloride was applied to the SPCE and incubated in dark. Next, 50 µL of BSA was added to prevent non-specific binding of antibody. Each step was incubated for 10 minutes and the SPCE was washed by dipping once in 5 mL of DI water after each step.

[Figure 1]

To test the sensitivity of the fabricated genosensor, different dilutions of *H5* viral gene DNA were applied onto the SPCE. Briefly, 5 µL of biotin- and fluorescein-labelled DNA was

pipetted onto the SPCE and incubated for 5 minutes. The biotin label will form specific covalent bond with streptavidin and hence the DNA was bound onto the SPCE. The SPCE was then incubated for 5 minutes with 5 µL of HRP-conjugated antifluorescein antibody. The antifluorescein antibody will bind to the fluorescein label on the DNA and thus the HRP enzyme was bound onto the SPCE. After each incubation step, the SPCE was washed by dipping 10 times in 5 mL of 0.1x SSC containing 0.5% SDS to minimize nonspecific immobilization of biological compound.

2.10 Amperometric Detection of H5 Gene

TMB substrate peroxidase solution (3,3',5,5'-Tetramethylbenzidine, 50 µL) (KPL, Gaithersburg, MD) was applied onto the fabricated genosensor for amperometric detection of polymerase chain reaction (PCR) amplicon derived from the haemagglutinin, *H5* gene of the highly pathogenic avian influenza (HPAI). The enzymatic redox reaction was detected as current signals using µAutolab PGSTAT III potentiostat (Metrohm, Netherlands) interfaced with controlling software NOVA 1.10. Intermittent pulse amperometry (IPA) was employed for the measurement in this study.

The *H5* PCR amplicon was serially diluted as shown in Table 1 to test the sensitivity of the genosensor. The reproducibility of the fabricated genosensor was determined by the relative standard deviation (%RSD) of three measurements performed in three separate experiments, which were calculated using standard deviations (SD) and mean current changes of the serially-diluted *H5* PCR amplicons. The threshold limits were set at 8.71 ± 0.87 µA, to generate a standard measurement.

[Table 1]

The data was assessed via Shapiro-Wilk test and Bartletts's test, respectively in Genstat to determine the distribution pattern of the residuals and homogeneity of variance. One-way analysis of variance (ANOVA) was used to evaluate the performance of G/ZnO/PSE-

modified SPCE at different concentrations. Differences were considered significant at $P < 0.05$.

3. Results and Discussion

3.1 Characterisation of graphene/ZnO nanocomposite

In this study, the approach employed for the synthesis of G/ZnO nanocomposite is facile and environmental friendly. The morphology of the G/ZnO nanocomposite was analysed using FESEM as shown in Figure 2A. The ZnO nanoparticles formed on the graphene sheet were spherical in shape with diameter around 200 nm. It was also observed that the ZnO nanoparticles were well distributed on the graphene sheets. TEM analysis was performed to supplement the evidence of exfoliation of graphite and formation of ZnO on the graphene sheets as indicated in Figure 2B and 2C, respectively. The TEM results manifest the transparent nature of the graphene indicating graphite was exfoliated into thin sheets and deposition of ZnO nanoparticles on the surface of the graphene sheets.

The formation of ZnO nanoparticles from precursor can be illustrated from Equation (1), (2) and (3). Sodium hydroxide (NaOH) reacts rapidly with zinc nitrate hexahydrate ($Zn(NO_3)_2 \cdot 6H_2O$) to generate $Zn(OH)_2$ colloids as shown in Equation 1, part of the $Zn(OH)_2$ dissolves into Zn^{2+} and OH^- ions during the process as indicated in Equation 2. Lastly, ZnO nuclei are formed when concentration of the ions reaches supersaturation degree of ZnO according to Equation 3. The ZnO nuclei grow larger along the planes and edges of graphene sheets to form the nanocomposites.

$$Zn(NO_3)_2 \cdot 6H_2O + 2NaOH \Rightarrow Zn(OH)_2 + 2NaNO_3 + 6H_2O \quad \text{Equation (1)}$$

$$Zn(OH)_2 + 2H_2O \Rightarrow Zn^{2+} + 2OH^- + 2H_2O \Rightarrow Zn(OH)_4^{2-} + 2H^+ \quad \text{Equation (2)}$$

$$Zn(OH)_4^{2-} \Rightarrow ZnO + H_2O + 2OH^- \quad \text{Equation (3)}$$

In general, a larger ZnO crystal is a polar crystal whose positive polar plane is rich in Zn and the negative polar plane is rich in O. In the hydrothermal growth process, the growth unit of

ZnO is $[Zn(OH)_4]^{2-}$, which leads to different growth rate of planes as reported by Wu and colleagues [16]. The growth rates of different planes are shown as follows:

$$V(0001) > V(01\bar{1}\,\bar{1}) > V(01\bar{1}\,0) > V(01\bar{1}\,1) > V(000\bar{1})$$

Plane disappears quicker as the growth rate increases [17]. Therefore, the most rapid growth rate plane will disappear in the hydrothermal growth process, leading to the formation of rod-like shape ZnO nanoparticles. However, at high reaction temperature (more than 90 ℃), heat convection, deregulation movement among molecules and ions in the solution become intense and the deposit rate of the growth unit $[Zn(OH)_4]^{2-}$ on ZnO nuclei became more rapid. Referring to the growth rule mentioned, the second rapid growth rate plane, $(01\bar{1}\,1)$ may be grown slower than $(01\bar{1}\,0)$ plane. Therefore, the $(01\bar{1}\,0)$ plane extrudes and displays as quasi-spherical particles, as shown in Figure 2C.

The chemical composition of the as-synthesised product was analysed via energy dispersive X-ray spectrometry (EDAX). The peaks of C, O and Zn in the spectrum depict the presence of carbon, oxygen and zinc compound only, thereby further affirming the purity of the product. The peak corresponding to silicon (Si) was due to the specimen being drop casted onto silicon substrate for characterisation.

[Figure 2]

The XRD patterns of the raw graphite, as-exfoliated graphene, ZnO and as-synthesised G/ZnO nanocomposites are shown in Figure 3. The diffraction peaks at 26.63° and 54.71° for graphite and graphene are similar, accounting for the graphitic reflection of (002) plane, which correspond to a *d*-spacing of 3.34Å (ICSD no. 98-005-2916). This result indicated that the sonochemical method employed for the exfoliation of graphite did not disrupt the pristine crystalline structure, preserving the intact lattice structure of the exfoliated graphene. This differs from graphene synthesised via chemical routes which involves reduction through harsh acid mixture that culminates in structural defects, affecting the properties of the materials. The peaks at 2θ = 32.07°, 34.80°, 36.55°, 47.80°, 56.88°, 63.14°, 66.74° and

68.26 can be indexed to the characteristic ZnO crystal planes of (001), (400), (201), (401), (540), (601), (112) and (631), respectively, corresponding to the wurtzite hexagonal structure of ZnO (ICSD no. 98-006-5172). The XRD pattern affirms that the synthesis method employed retained the crystallographic structure of both graphene and ZnO. In addition, no other diffraction peak was observed, confirming the purity of the as-synthesised G/ZnO nanocomposite.

[Figure 3]

Raman spectroscopy is an effective nanometrology analysis method for investigating the crystallisation, structure and defect in nanomaterial. The Raman spectra of graphene and G/ZnO nanocomposite are shown in Figure 4. For graphene, three distinct features are prominent, namely the G band at ~1580 cm^{-1} which corresponds to the in-plane vibration of sp^2 carbon atoms, the 2D band at 2719 cm^{-1} and the D band at 1351 cm^{-1}, ascribing to the first-order zone boundary phonons. The D peak is typically associated with edge defects, in which the formation of new edges from the exfoliation process of graphite can be seen as defects [18]. Four peaks labelled as “Z” appeared after the hydrothermal treatment, indicating the growth of ZnO nanoparticles. The peak at ~432 cm^{-1} corresponds to the finger signal of the characteristic E_2 mode of ZnO wurtzite structure, while the peaks at ~327 and ~574 cm^{-1} are well indexed to the transversal optical modes with A_1 symmetry and the longitudinal optical (LO) modes [19]. The broad peak at ~1127 cm^{-1} is attributed to 2A1 (LO), 2E1 (LO) and 2LO mode of ZnO [20]. The D-band, G-band and 2D-band were located at ~1349 cm^{-1}, ~1574 cm^{-1} and ~2717 cm^{-1}, the shift of the bands are likely due to the doping effects of ZnO [21]. The Raman spectrum after the hydrothermal treatment confirms that the structure of graphene was not destroyed and the G/ZnO nanocomposites were formed, which is in good agreement with the XRD results (Figure 3).

[Figure 4]

3.2 Electrochemical response of graphene/ZnO nanocomposite-modified SPCE

Cyclic voltammetry (CV) was performed to discern the role of individual component and possible synergy between the composite. CV was carried out in PBS buffer (pH 7.4) containing 1 mM of H_2O_2 at a scan rate of 50 mV/s in the potential range of -0.4 V to 0.8 V. Based on Figure 5, both graphene (curve b) and G/ZnO nanocomposite-modified SPCE (curve c) showed an enhanced activity towards the reduction of H_2O_2 as compared to that of bare SPCE (curve a). The results also depicted that the G/ZnO nanocomposite (curve c) demonstrated significant increase in peak current of almost 3 times of the response of bare SPCE (curve a). The improved electrochemical properties of the nanocomposites could be attributed to the synergistic effect between graphene and ZnO nanoparticles, in which the pristine quality of the graphene improves the electrical conductivity while ZnO nanoparticles provide a 3D conductive system for the transfer of electron [10].

Hydrogen peroxide (H_2O_2) is generally taken as the model analyte for the evaluation and electroanalytical properties of materials since it is the by-product of most electrochemical response of enzymatic process and also plays an important role in food industry, environmental monitoring, clinical diagnosis and detection of biological compounds [22]. Therefore, the sensitivity of a biosensor towards the detection of H_2O_2 is of utmost importance. In Figure 5(d), the CV response of G/ZnO nanocomposite-modified SPCE increased dramatically upon the addition of H_2O_2, revealing remarkable electrocatalytic activity of the composite towards the reduction of H_2O_2. This can be attributed to the large surface area-to-volume ratio of graphene and electroactive property of ZnO, thus improving the electron transfer process [10]. Notably, no redox peaks were observed in Figure 5(d), since the redox peaks for H_2O_2 occurs at very high switching potential [23]. Therefore, it is due to this reasoning that non-enzymatic H_2O_2 biosensor is assessed at the maximum current to ascertain its sensing capability [24].

[Figure 5]

3.3 Effect of Scan Rate

Figure 6 shows the cyclic voltammograms recorded for G/ZnO nanocomposite-modified SPCE by varying scan rate from 10 to 100 mV/s. In general, it was observed in Figure 6 that peak current increased when a faster scan rate is used. According to the Randles-Sevcik equation (Eq. 4), in a Nernstian system (reversible system), linear relationship between peak current (i_p) and square root of scan rate ($v^{1/2}$) provides evidence for a chemically reversible and controlled diffusion electrochemical process [25].

$$i_p = (2.69 \times 10^5)\, n^{3/2} A D^{1/2} C v^{1/2} \qquad \text{Equation (4)}$$

At 25 ℃, i_p is the peak current (A), n is the electron stoichiometry, A is the electrode area (cm^2), D is the diffusion coefficient (cm^2s^{-1}), C is the concentration ($molcm^{-3}$) and v is the scan rate (V/s).

[Figure 6]

It was observed that the occurrence of maximum peak currents always remained at the same voltage regardless of the value of scan rate applied, indicating reversible electron transfer kinetics of the electrode. Besides, the peak current is linearly proportional to the square root of the scan rate as seen in the inset of Figure 6, with a correlation coefficient, R^2 of 0.9781. This indicates a diffusion controlled process of the reactants, a relationship which reaffirms that measurements correlate to surface confined reactions at the electrode [25].

3.4 Amperometric Determination of H_2O_2 at Graphene/ZnO Nanocomposite-modified SPCE

Amperometry is an analytical chemistry technique to evaluate the sensor's electrocatalytic activity towards the analyte by measuring the current in an electrochemical cell at a fixed potential. In the present study, the electrochemical performance of the as-synthesised G/ZnO nanocomposite was evaluated using the amperometric technique with H_2O_2. This is essential since further development of the sensing platform into genosensor works on the basis of H_2O_2 detection. During the amperometric *i-t* measurements, the working potential was set at -0.4 V, where the amperometric response of the modified SPCE reached the maximum value. For every 50 seconds, aliquots of 1 mM H_2O_2 were successively injected

into the PBS buffer. For performance comparison purpose, similar analyses were carried out using bare and graphene-modified SPCE.

The amperometric *i-t* responses of bare, graphene- and G/ZnO nanocomposite-modified SPCE are shown in Figure 7. It was observed that upon the successive addition of 1 mM H_2O_2, the G/ZnO nanocomposite-modified SPCE displayed highest current response as compared to bare and graphene-modified SPCE. The G/ZnO nanocomposite-modified SPCE responded rapidly and reached a steady state (95% of the maximum value) within 3 seconds, indicating a fast amperometric response to H_2O_2 reduction and the high sensitivity of the biosensor.

[Figure 7]

In addition, the G/ZnO nanocomposite-modified SPCE displayed good linear relationship with H_2O_2 in the range of 1 to 15 mM with a correlation coefficient, R^2 of 0.9977 (Figure 7 inset). It was also observed that G/ZnO nanocomposite-modified SPCE exhibited the highest sensitivity (3.2580 μAmM^{-1}) among the three SPCEs tested, approaching approximately 200% current response of bare SPCE (1.6709 μAmM^{-1}). The detection limit of the G/ZnO nanocomposite-modified SPCE was estimated to be 7.4357 µM based on signal-to-noise ratio equal to 3 (S/N = 3).

The analysis on the ANOVA, means and standard deviations are presented in Table 2 and Figure 7 inset. The one-way ANOVA showed significant main effect for sensor modified with different materials, $F(2, 42) = 8.35$, $P < 0.05$. From the Fisher's protected least significant difference (LSD) analysis, it was observed that the G/ZnO nanocomposite-modified SPCE showed the highest significance for the sensitivity for the detection of H_2O_2 as indicated by the letter "a" in Figure 7 inset.

[Table 2]

Table 3 shows the comparison of several typical nonenzymatic H_2O_2 sensors reported previously, the present graphene/ZnO-modified sensor displayed comparable performance.

The high sensitivity of the G/ZnO nanocomposite based sensing platform is promising and is postulated to be suitable for the detection of other biological compounds, such as glucose, DNA as well as biomarkers.

[Table 3]

The selectivity of the graphene/ZnO-modified SPCE was studied by introducing common interference species into the PBS buffer. Figure 8 shows the amperometric response upon the addition of 1 mM uric acid, 1 mM fructose and 1 mM glucose into the buffer. The result demonstrates that for each addition of H_2O_2, the graphene/ZnO-modified sensor showed quick response. On the other hand, no obvious response was observed for the addition of 1 mM uric acid, fructose and glucose respectively. The result validates the high selectivity of graphene/ZnO-modified SPCE towards the detection of H_2O_2.

[Figure 8]

3.5 Electrochemical Detection of H5 Gene at Graphene/ZnO Nanocomposite Enhanced Biosensor

The amperometric response of G/ZnO/PSE-modified SPCE with different dilutions of *H5* PCR product is shown in Figure 9. After serial testing of no template and buffer negative controls, the threshold limit for G/ZnO/PSE-modified SPCE was set at 8.71 ± 0.87 μA to discriminate between positive and negative samples. The accuracy of the electrochemical genosensor for the *H5* PCR product was assessed by comparing the samples according to the threshold limit. The G/ZnO-enhanced genosensor displayed high accuracy in the detection of positive samples (above threshold value) and negative controls (below threshold value) as depicted in Figure 9. It was also observed that the current response was concentration-dependent. The increase of the dilution factor of PCR amplicon resulted in decreasing current response. This decrease in response is due to lower amount of binding sites available for the attachment of anti-fluorescein labelled HRP in the sandwich platform (Figure 1). The H_2O_2 binding to HRP oxides the heme iron ion in the catalytic site, TMB

substrate then binds to the catalytic site and is oxidised to release electron [26]. Therefore, reduction of binding sites and release of electron have led to lower current signal generation.

[Figure 9]

The analysis on the ANOVA, means and standard deviations are presented in Table 4 and Figure 9. The one-way ANOVA showed significant main effect for dilution factor, $F(5, 12) = 12.29$, $P < 0.05$. From the Fisher's protected LSD analysis, it was observed that the G/ZnO nanocomposite-enhanced genosensor showed the highest significance for the detection of non-diluted *H5* PCR amplicon than other diluted PCR amplicons as indicated by the letter "a" in Figure 9.

[Table 4]

Dot blot assay was performed to investigate the feasibility of the sensing platform, where TMB acts the visualising reagent for the observation of colorimetric change. As observed in Figure 10, increasing the dilution factor of the PCR amplicon resulted in a decrease in dot intensity, while negative control displayed no colorimetric response. This is due to higher dilution factor possesses lower amount of fluorescein-labelled PCR amplicon for the binding of anti-fluorescein HRP, resulting in lesser redox reactions of TMB and H_2O_2, leading to lower blue intensity observed in the dot blot assay. The dot blot assay proved the feasibility of the sensing platform and the result obtained is in agreement with that of G/ZnO nanocomposite-enhanced genosensor, thereby complementing the genosensing assay.

[Figure 10]

The detection of *H5* PCR amplicon by G/ZnO nanocomposite-enhanced genosensor was compared with the conventional method for PCR amplicon detection, agarose gel electrophoresis. The fluorescence signals observed from gel electrophoresis for PCR product subjected to dilution factor of 1, 2, 4, 8, 16 and 32 (L1-L6) were shown in Figure 11. The band sizes of the PCR amplicons in Figure 10 are slightly larger than the 1500 bp ladder indicator, corresponding to the size of *H5* gene (1616 bp), thereby affirming successful PCR

amplification of targeted *H5* gene sequence. The fluorescence signals obtained were in agreement with the current signals detected by the genosensor, in which the signals weakened with increasing dilution factors. No obvious fluorescence signal was observed for PCR samples with dilution factors of 8 and above. On the other hand, the current response of the G/ZnO/PSE-enhanced genosensor was still significant ($P < 0.05$) when the PCR amplicon was diluted to $^{1}/_{32}$ (Figure 9), exhibiting approximately 5 times better sensitivity than the conventional gel electrophoresis. Furthermore, genosensor also displayed the advantages of short detection duration, low sample consumption, exclusion of carcinogenic agent (UV light and ethidium bromide) and generation of quantifiable result as compared to gel electrophoresis.

[Figure 11]

4. Conclusion

In summary, a facile green approach for the synthesis of graphene/ZnO nanocomposite has been developed. G/ZnO nanocomposite was synthesised in a green and facile method, with safer procedure as it eliminates the need of harsh chemical and high temperature incubation. The SEM and TEM images revealed that ZnO nanoparticles were homogenously distributed on the graphene sheets while XRD result affirmed the successful hydrothermal growth of ZnO nanoparticles.

The G/ZnO nanocomposite was functionalised with PSE, a bi-linker consisting of a pyrene moiety and a succinimidyl fragment, for the attachment of biological compound. This simple organic bi-linker enables strong irreversible non-covalent bonding to the surface of graphene via π- π hydrophobic stacking that does not disrupt the pristine structure of graphene while succinimidyl ester at the other end allows the bonding to amine groups on any biological surface [15]. In addition, the pyrene and succinimidyl fragments are connected in PSE by an alkyl chain whose structure is highly flexible, thereby developing a highly versatile sensing platform based on G/ZnO nanocomposite [27].

The graphene/ZnO nanocomposite-modified SPCE exhibited excellent electrocatalytic activity towards H_2O_2 due to the good electrical conductivity of graphene and good electroactive property of ZnO. The graphene/ZnO nanocomposite enhanced electrochemical DNA biosensor also displayed good sensitivity towards the detection of *H5* gene PCR amplicon, showing a proof of concept which can be investigated further for the development of an early and rapid detection tool for the avian influenza H5N1 virus. In addition, the PCR amplicon denaturation and hybridisation steps typically employed in a conventional electrochemical genosensor assay have been eliminated with the specific labelling of PCR amplicon with biotin and fluorescein. This G/ZnO nanocomposite-enhanced electrochemical DNA biosensor enables safe, rapid, sensitive and efficient detection of *H5* gene PCR amplicon as compared to the conventional agarose gel electrophoresis. Although this present assay was designed specifically for *H5* DNA detection, the G/ZnO nanocomposite enhanced sensing platform can also be used for detection of other biological molecules using antigen-antibody interaction. Future replacements on nucleic acid amplification and usage of portable reader can make point-of-care testing possible with the graphene/ZnO nanocomposite enhanced sensing platform.

Acknowledgments

Financial support from the Ministry of Higher Education (FRGS grant code: FRGS/2/2014/SG06/UNIM/03/1), HIR-Chancellory UM (UM.C/625/1/HIR/079), HIR-MOHE (UM.C/625/1/HIR/MOHE/SC/06) and the University of Nottingham are gratefully acknowledged.

References

[1] H. Hosseini, M. Behbahani, M. Mahyari, H. Kazerooni, A. Bagheri, A. Shaabani, Ordered carbohydrate-derived porous carbons immobilized gold nanoparticles as a new electrode material for electrocatalytical oxidation and determination of nicotinamide adenine dinucleotide, Biosens. Bioelectron. 59 (2014) 412-417.
[2] K.S. Novoselov, A.K. Geim, S.V. Morozov, D. Jiang, Y. Zhang, S.V. Dubonos, I.V. Grigorieva, A.A. Firsov, Electric field effect in atomically thin carbon films, Science 306 (2004) 666-669.
[3] M. Pumera, Graphene in biosensing, Mater. Today 14 (2011) 308-315.

[4] B.N. Joshi, H. Yoon, S.-H. Na, J.-Y. Choi, S.S. Yoon, Enhanced photocatalytic performance of graphene–ZnO nanoplatelet composite thin films prepared by electrostatic spray deposition, Ceram. Int. 40 (2014) 3647-3654.
[5] R.R. Salunkhe, Y.-H. Lee, K.-H. Chang, J.-M. Li, P. Simon, J. Tang, N.L. Torad, C.-C. Hu, Y. Yamauchi, Nanoarchitectured graphene-based supercapacitors for next-generation energy-storage applications, Chemistry – A European Journal 20 (2014) 13838-13852.
[6] K. Anand, O. Singh, M.P. Singh, J. Kaur, R.C. Singh, Hydrogen sensor based on graphene/ZnO nanocomposite, Sensors Actuators B: Chem. 195 (2014) 409-415.
[7] R.-J. Chung, Z.-C. Lin, P.-K. Yang, K.-Y. Lai, S.-F. Jen, P.-W. Chiu, Hybrid ZnO NR/graphene structures as advanced optoelectronic devices with high transmittance, Nanoscale Res Lett 8 (2013) 1-5.
[8] Q. Ouyang, Z. Xu, Z. Lei, H. Dong, H. Yu, L. Qi, C. Li, Y. Chen, Enhanced nonlinear optical and optical limiting properties of graphene/ZnO hybrid organic glasses, Carbon 67 (2014) 214-220.
[9] Y. Zhu, H.I. Elim, Y.L. Foo, T. Yu, Y. Liu, W. Ji, J.Y. Lee, Z. Shen, A.T.S. Wee, J.T.L. Thong, C.H. Sow, Multiwalled carbon nanotubes beaded with ZnO nanoparticles for ultrafast nonlinear optical switching, Adv. Mater. 18 (2006) 587-592.
[10] S. Palanisamy, S.-M. Chen, R. Sarawathi, A novel nonenzymatic hydrogen peroxide sensor based on reduced graphene oxide/ZnO composite modified electrode, Sensors Actuators B: Chem. 166–167 (2012) 372-377.
[11] T. Lu, Y. Zhang, H. Li, L. Pan, Y. Li, Z. Sun, Electrochemical behaviors of graphene–ZnO and graphene–SnO2 composite films for supercapacitors, Electrochim. Acta 55 (2010) 4170-4173.
[12] A. Ali, K. Ali, K.-R. Kwon, M. Hyun, K. Choi, Electrohydrodynamic atomization approach to graphene/zinc oxide film fabrication for application in electronic devices, J Mater Sci: Mater Electron 25 (2014) 1097-1104.
[13] J.S.Y. Chia, M.T.T. Tan, P.S. Khiew, J.K. Chin, H. Lee, D.C.S. Bien, W.S. Chiu, A novel one step synthesis of graphene via sonochemical-assisted solvent exfoliation approach for electrochemical sensing application, Chem. Eng. J. 249 (2014) 270-278.
[14] E.R. Ezeigwe, M.T.T. Tan, P.S. Khiew, C.W. Siong, One-step green synthesis of graphene/ZnO nanocomposites for electrochemical capacitors, Ceram. Int. 41 (2015) 715-724.
[15] J.S.Y. Chia, M.T.T. Tan, P.S. Khiew, J.K. Chin, C.W. Siong, A bio-electrochemical sensing platform for glucose based on irreversible, non-covalent pi–pi functionalization of graphene produced via a novel, green synthesis method, Sensors Actuators B: Chem. 210 (2015) 558-565.
[16] C. Wu, X. Qiao, J. Chen, H. Wang, F. Tan, S. Li, A novel chemical route to prepare ZnO nanoparticles, Mater. Lett. 60 (2006) 1828-1832.
[17] W.-J. Li, E.-W. Shi, W.-Z. Zhong, Z.-W. Yin, Growth mechanism and growth habit of oxide crystals, J. Cryst. Growth 203 (1999) 186-196.
[18] A.C. Ferrari, D.M. Basko, Raman spectroscopy as a versatile tool for studying the properties of graphene, Nat. Nano. 8 (2013) 235-246.
[19] H. Zeng, Y. Cao, S. Xie, J. Yang, Z. Tang, X. Wang, L. Sun, Synthesis, optical and electrochemical properties of ZnO nanowires/graphene oxide heterostructures, Nanoscale Res Lett 8 (2013) 133.
[20] R. Cuscó, E. Alarcón-Lladó, J. Ibáñez, L. Artús, J. Jiménez, B. Wang, M.J. Callahan, Temperature dependence of Raman scattering in ZnO Phys. Rev. B 75 (2007) 165202.
[21] X. Dong, Y. Cao, J. Wang, M.B. Chan-Park, L. Wang, W. Huang, P. Chen, Hybrid structure of zinc oxide nanorods and three dimensional graphene foam for supercapacitor and electrochemical sensor applications, RSC Advances 2 (2012) 4364-4369.
[22] M.-J. Song, S. Hwang, D. Whang, Amperometric hydrogen peroxide biosensor based on a modified gold electrode with silver nanowires, J. Appl. Electrochem. 40 (2010) 2099-2105.
[23] M. Florescu, C.M.A. Brett, Development and evaluation of electrochemical glucose enzyme biosensors based on carbon film electrodes, Talanta 65 (2005) 306 - 312.

[24] C. Anjalidevi, V. Dharuman, J. Shankara Narayanan, Non enzymatic hydrogen peroxide detection at ruthenium oxide–gold nano particle–Nafion modified electrode, Sensors Actuators B: Chem. 182 (2013) 256-263.
[25] A.J. Bard, L.R. Faulkner, Potential Sweep Methods, 2nd, John Wiley & Sons, Inc., 2001.
[26] N.C. Veitch, Horseradish peroxidase: a modern view of a classic enzyme, Phytochemistry 65 (2004) 249-259.
[27] V.A. Karachevtsev, S.G. Stepanian, A.Y. Glamazda, M.V. Karachevtsev, V.V. Eremenko, O.S. Lytvyn, L. Adamowicz, Noncovalent Interaction of Single-Walled Carbon Nanotubes with 1-Pyrenebutanoic Acid Succinimide Ester and Glucoseoxidase, Journal of Physical Chemistry C 115 (2011) 21072-21082.
[28] X. He, C. Hu, H. Liu, G. Du, Y. Xi, Y. Jiang, Building Ag nanoparticle 3D catalyst via Na2Ti3O7 nanowires for the detection of hydrogen peroxide, Sensors Actuators B: Chem. 144 (2010) 289-294.
[29] L. Wang, E. Wang, A novel hydrogen peroxide sensor based on horseradish peroxidase immobilized on colloidal Au modified ITO electrode, Electrochem. Commun. 6 (2004) 225-229.
[30] M. Liu, R. Liu, W. Chen, Graphene wrapped Cu2O nanocubes: Non-enzymatic electrochemical sensors for the detection of glucose and hydrogen peroxide with enhanced stability, Biosens. Bioelectron. 45 (2013) 206-212.
[31] S.A.G. Evans, J.M. Elliott, L.M. Andrews, P.N. Bartlett, P.J. Doyle, G. Denuault, Detection of Hydrogen Peroxide at Mesoporous Platinum Microelectrodes, Anal. Chem. 74 (2002) 1322-1326.

Figure Captions

Fig. 1. Schematic diagram for the development of G/ZnO nanocomposite enhanced electrochemical DNA biosensor on SPCE for the detection of *H5* gene.

Fig. 2. SEM image of (A) G/ZnO nanocomposite, TEM images of (B) graphene, (C) G/ZnO nanocomposite, EDAX analysis of (D) G/ZnO nanocomposite.

Fig. 3. XRD patterns of graphite, graphene, zinc oxide and G/ZnO nanocomposite.

Fig. 4. Raman spectra of graphene and G/ZnO nanocomposite.

Fig. 5. Cyclic voltammograms of (a) bare SPCE, (b) graphene-modified SPCE, (c) G/ZnO nanocomposite-modified SPCE and (d) G/ZnO nanocomposite-modified SPCE in H_2O_2.

Fig. 6. Cyclic voltammograms of G/ZnO nanocomposite-modified SPCE at varying scan rates from 10 to 100 mV/s. Inset shows the linear dependence of peak current against square root of scan rates.

Fig. 7. Real time amperometric response of bare, graphene- and G/ZnO nanocomposite-modified SPCE for successive additions of H_2O_2 ranging from 1 to 15 mM in PBS buffer at a fixed potential of -0.4 V.

Fig. 8. Amperometric response of graphene/ZnO nanocomposite-modified SPCE for the successive addition of 1 µM H_2O_2, 1 mM uric acid, 1 mM fructose, 1 mM glucose and 1 µM H_2O_2 into PBS buffer.

Fig. 9. Amperometric response of G/ZnO nanocomposite-enhanced electrochemical DNA biosensor with different dilutions of *H5* PCR amplicon (mean ± SD (n=3)), error bars were plotted according to the SD of each triplicate, different letters indicate differences among dilution factors determined by Fisher's protected least significant difference (LSD) test at P = 0.05.

Fig. 10. Dot blot assay results for different dilutions of *H5* gene PCR amplicon.

Fig. 11. Agarose gel electrophoresis of *H5* PCR amplicons at different concentrations. Lad: 1 kbp DNA ladder; L1-L6: PCR products with different dilution factors of 1, 2, 4, 8, 16 and 32, respectively; L7: negative control.

Table Captions

Table 1. Dilution factor of *H5* PCR amplicon and their respective concentrations.

Table 2. Results of one-way analysis of variance (ANOVA) with sensor at 3 levels in a completely randomised design (CRD).

Table 3. Comparison of graphene/ZnO-modified electrode with some previously reporter H_2O_2 sensors.

Table 4. Results of one-way analysis of variance (ANOVA) with dilution factor at 6 levels replicated 3 times in a completely randomised design (CRD).

[Figure 1]

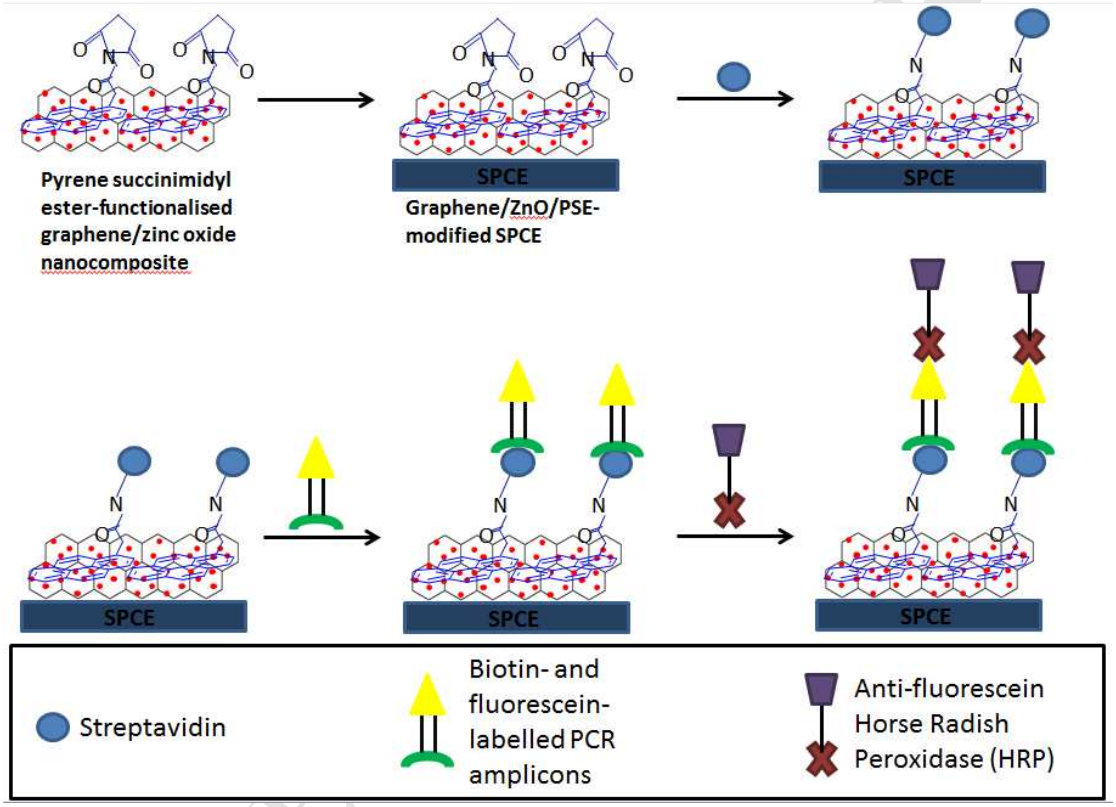
Pyrene succinimidyl ester-functionalised graphene/zinc oxide nanocomposite
SPCE
Graphene/ZnO/PSE-modified SPCE
SPCE
SPCE
SPCE
SPCE
Streptavidin
Biotin- and fluorescein-labelled PCR amplicons
Anti-fluorescein Horse Radish Peroxidase (HRP)

[Figure 2]

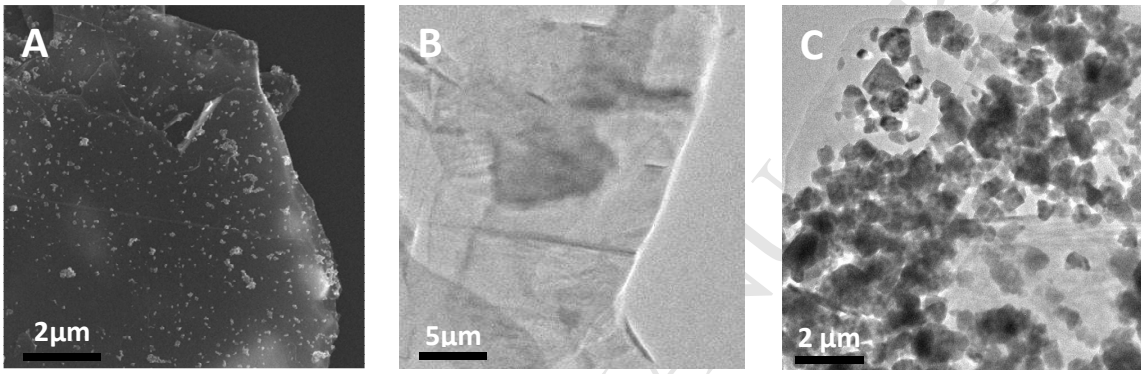
A
2µm
B
5µm
C
2 µm

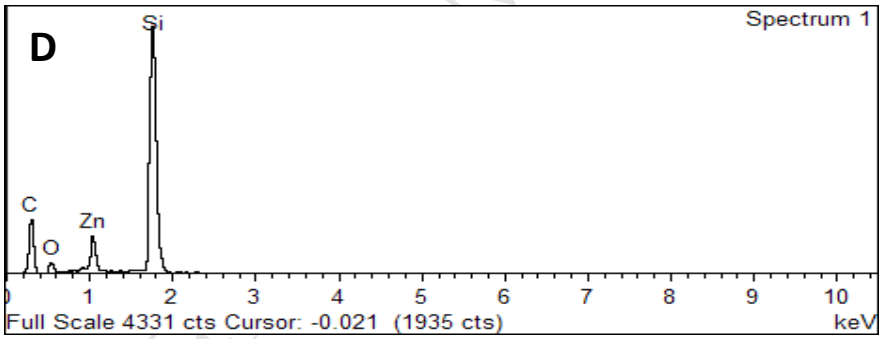
D
Spectrum 1
Si
C
O
Zn
0
1
2
3
4
5
6
7
8
9
10
Full Scale 4331 cts Cursor: -0.021 (1935 cts)
keV

[Figure 3]

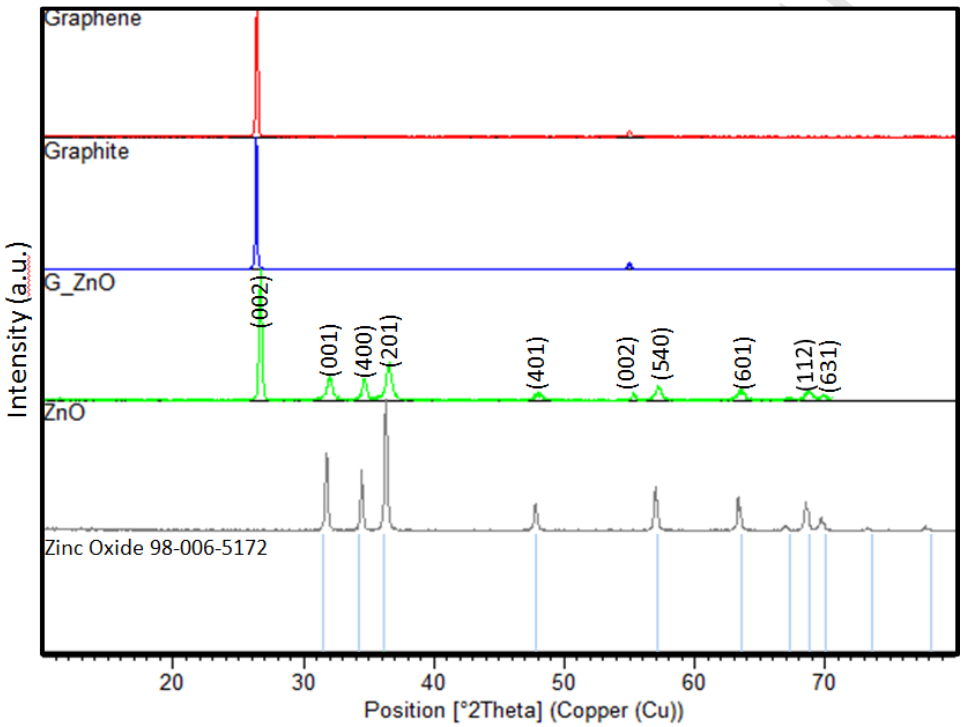
Graphene
Graphite
G_ZnO
ZnO
Zinc Oxide 98-006-5172
(002)
(001)
(400)
(201)
(401)
(002)
(540)
(601)
(112)
(631)
Intensity (a.u.)
20
30
40
50
60
70
Position [°2Theta] (Copper (Cu))

[Figure 4]

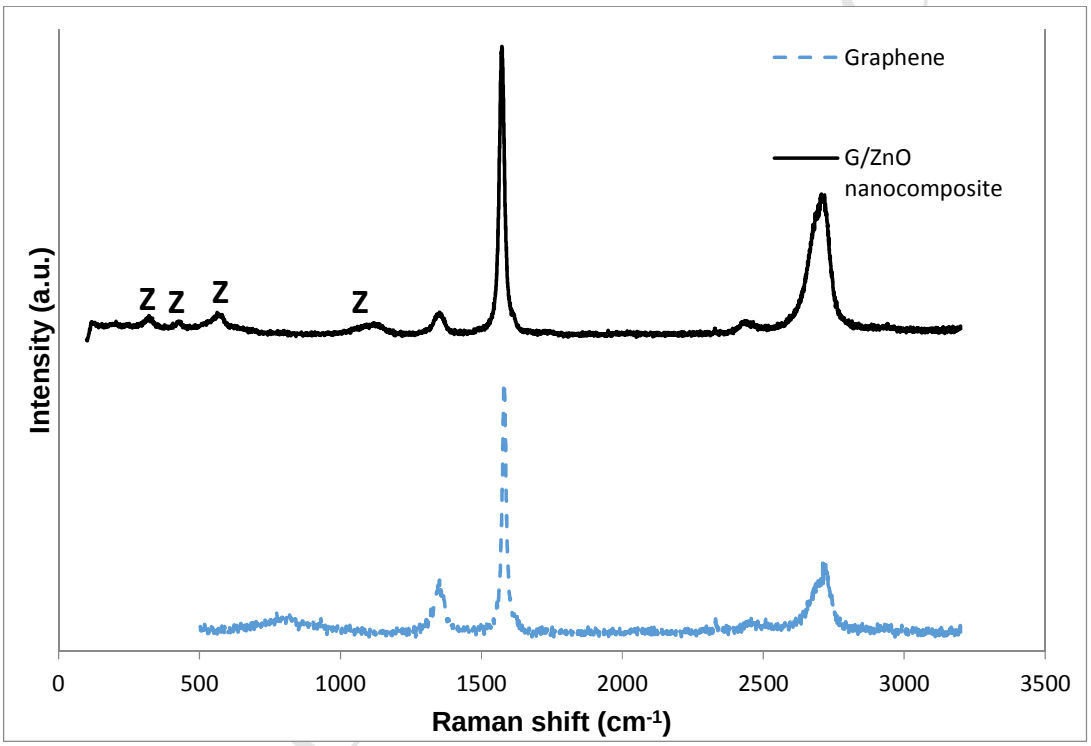
Graphene
G/ZnO nanocomposite
Z
Z
Z
Z
Intensity (a.u.)
0
500
1000
1500
2000
2500
3000
3500
Raman shift (cm-1)

[Figure 5]

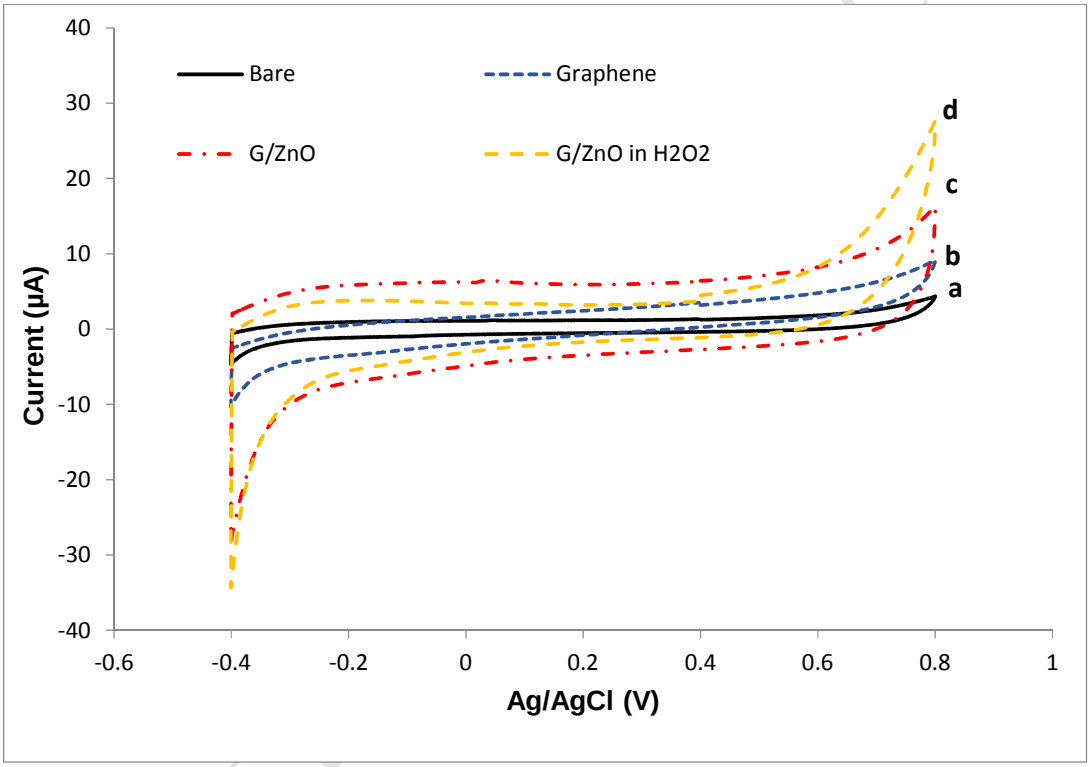
Bare
Graphene
G/ZnO
G/ZnO in H2O2
a
b
c
d
Current (µA)
Ag/AgCl (V)
40
30
20
10
0
-10
-20
-30
-40
-0.6
-0.4
-0.2
0
0.2
0.4
0.6
0.8
1

[Figure 6]

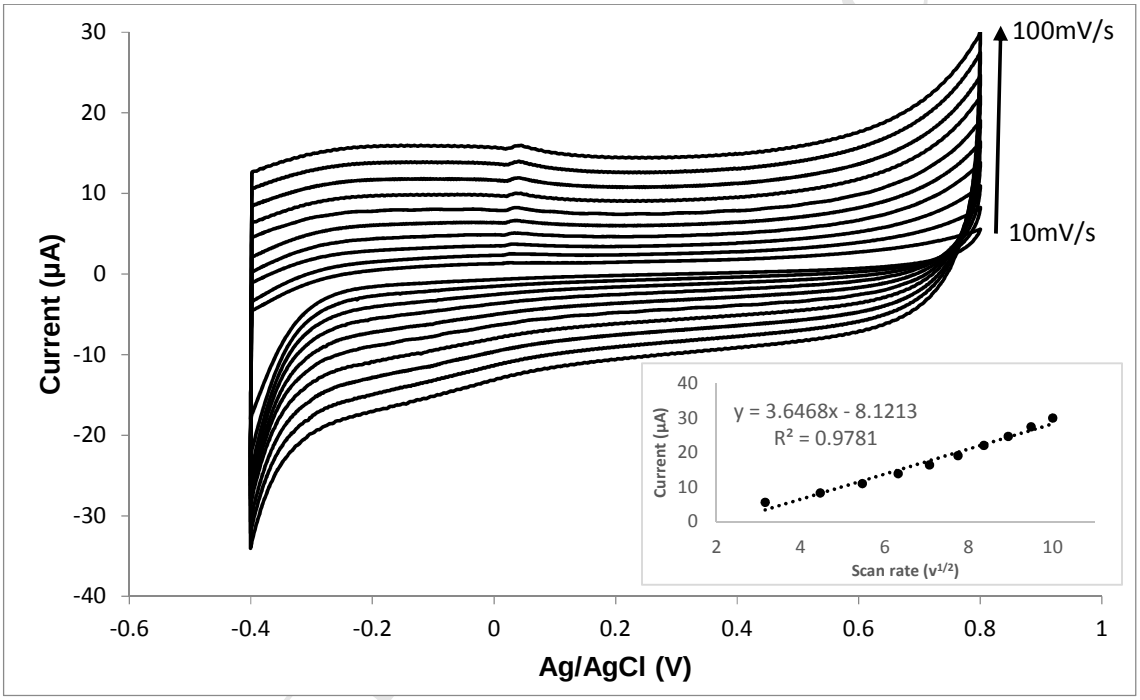
100mV/s
10mV/s
Current (µA)
Ag/AgCl (V)
30
20
10
0
-10
-20
-30
-40
-0.6
-0.4
-0.2
0
0.2
0.4
0.6
0.8
1
y = 3.6468x - 8.1213
R² = 0.9781
Current (µA)
Scan rate (v^1/2)
40
30
20
10
0
2
4
6
8
10

[Figure 7]

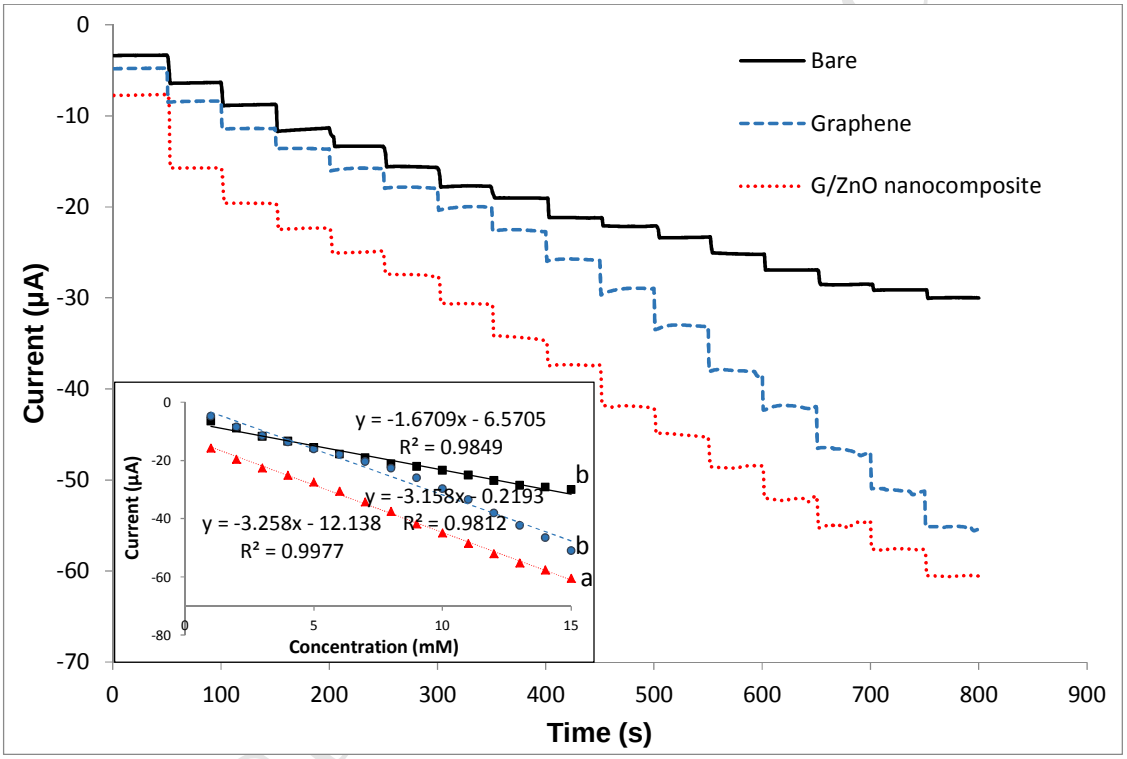
Bare
Graphene
G/ZnO nanocomposite
Current (µA)
Time (s)
0
-10
-20
-30
-40
-50
-60
-70
0
100
200
300
400
500
600
700
800
900
y = -1.6709x - 6.5705
R² = 0.9849
y = -3.158x - 0.2193
R² = 0.9812
y = -3.258x - 12.138
R² = 0.9977
b
b
a
Concentration (mM)
0
5
10
15
-80

[Figure 8]

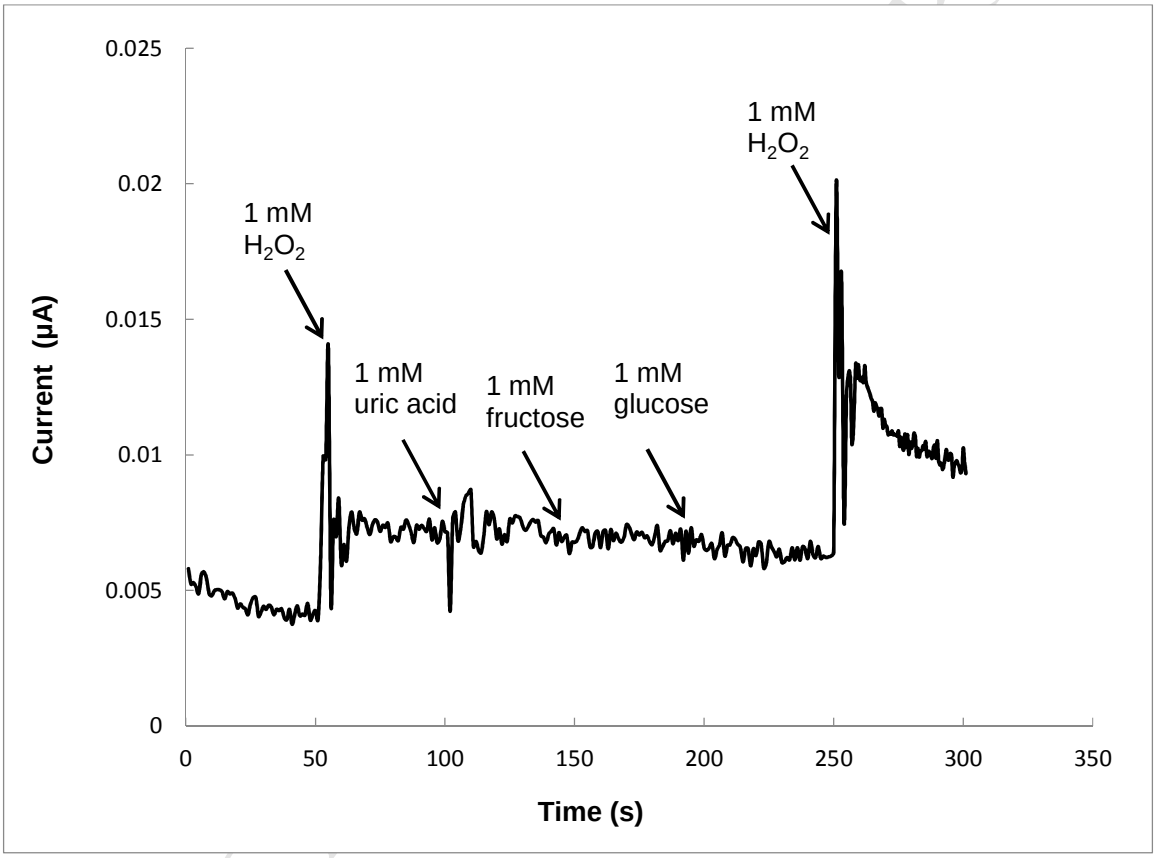
0.025
0.02
0.015
0.01
0.005
0
Current (μA)
0
50
100
150
200
250
300
350
Time (s)
1 mM H2O2
1 mM uric acid
1 mM fructose
1 mM glucose
1 mM H2O2

[Figure 9]

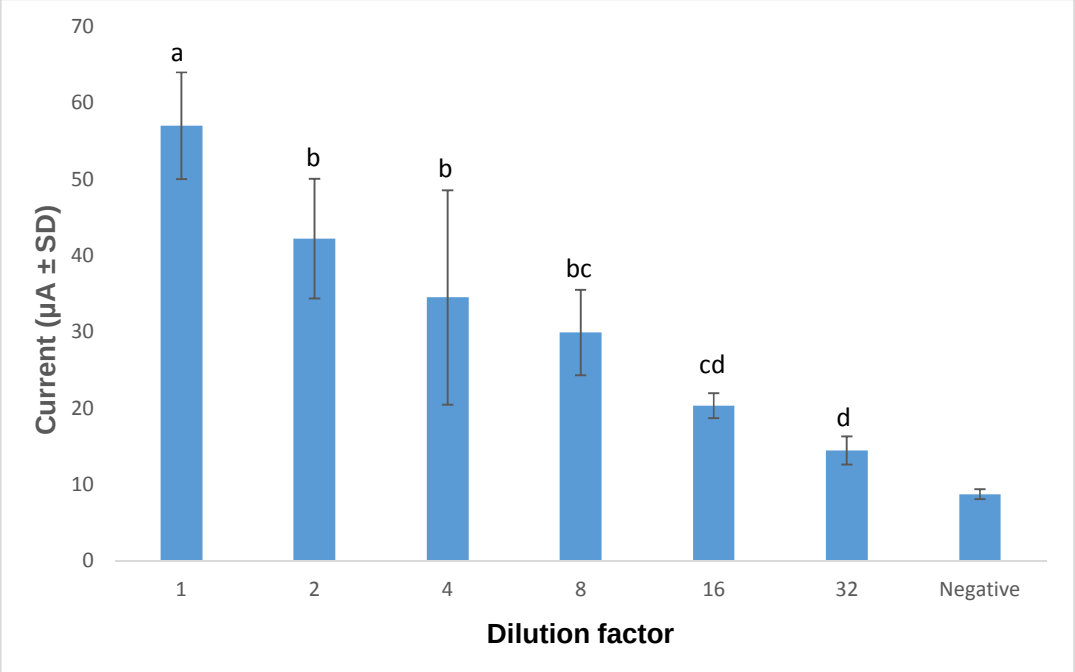

[Figure 10]

	Non-diluted PCR amplicon	$^1/_2$ diluted PCR amplicon	$^1/_4$ diluted PCR amplicon	$^1/_8$ diluted PCR amplicon	$^1/_{16}$ diluted PCR amplicon	$^1/_{32}$ diluted PCR amplicon	Negative control
Dot Blot Assay	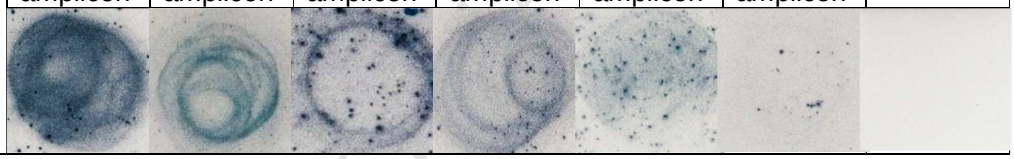						

[Figure 11]

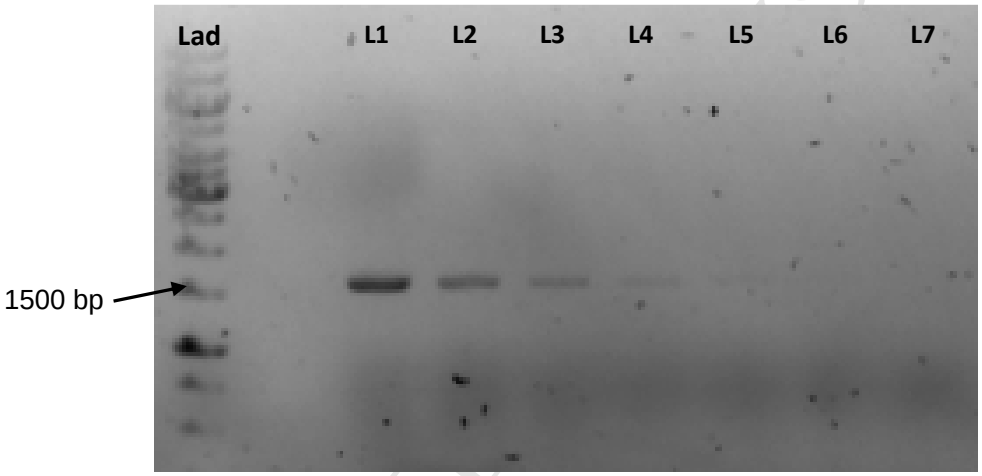

[Table 1]

Dilution factor	Concentration (ng/μL)
1	8.5096
2	4.2548
4	2.1274
8	1.0637
16	0.5319
32	0.2659

[Table 2]

Source of variation	Degree of freedom	Sum of square	Mean square	Computed F value	Probability value
Sensor	2	2.630×10^{-9}	1.315×10^{-9}	8.35	<.001
Residual	42	6.619×10^{-9}	1.576×10^{-10}		
Total	44	9.249×10^{-9}			

[Table 3]

Sensors	Detection limit	Sensitivity	Reference
Ag nanoparticles/graphite substrate	1.0 µM	0.0490 $\mu AmM^{-1}cm^{-2}$	[28]
Horseradish peroxidase/Au/ITO	8 µM	-	[29]
Graphene wrapped Cu_2O nanocubes	20.8 µM	-	[30]
Mesoporous platinum microelectrodes	4.5 µM	0.0028 $\mu AmM^{-1}cm^{-2}$	[31]
Graphene/ZnO	7.4357 µM	3.2580 μAmM^{-1}	This work

[Table 4]

Source of variation	Degree of freedom	Sum of square	Mean square	Computed F value	Probability value
Dilution factor	5	3.537×10^{-9}	7.073×10^{-10}	12.29	<.001
Residual	12	6.905×10^{-10}	5.754×10^{-11}		
Total	17	4.227×10^{-9}			

Highlights of Research

- ✓ One step, green and facile exfoliation of graphite in ethanol/water mixture.
- ✓ Graphene/ZnO nanocomposite prepared via simple, environmental friendly low temperature solvothermal method.
- ✓ Cyclic voltammetry and amperometric study of graphene/ZnO nanocomposite towards hydrogen peroxide with a good correlation coefficient of 0.9977.
- ✓ The nanocomposite exhibits enhanced electrochemical performances than the individual counterpart.
- ✓ Highly sensitive, rapid sensing platform was developed based on graphene/ZnO nanocomposite-enhanced screen-printed carbon electrode for the detection of *H5* PCR amplicon.